To be submitted to Journal of Applied Physics

Interface and thickness dependent domain switching and stability in Mg doped lithium niobate

Sabine M. Neumayer[1,2], Ilia N. Ivanov[3], Michele Manzo[4], Andrei L. Kholkin[5,6], Katia Gallo[4,a)] and Brian J. Rodriguez[1,2,a)]

[1]School of Physics, University College Dublin, Belfield, Dublin 4, Ireland

[2]Conway Institute of Biomolecular and Biomedical Research, University College Dublin, Belfield, Dublin 4, Ireland

[3]Center for Nanophase Materials Sciences, Oak Ridge National Laboratory, Oak Ridge, Tennessee, 37831, United States

[4]Department of Applied Physics, KTH - Royal Institute of Technology, Roslagstullbacken 21, 10691 Stockholm, Sweden

[5]Department of Physics & CICECO-Aveiro Institute of Materials, 3810-193 Aveiro, Portugal

[6]Institute of Natural Sciences, Ural Federal University, 620000 Ekaterinburg, Russia

a) Authors to whom correspondence should be addressed. Electronic addresses: brian.rodriguez@ucd.ie and gallo@kth.se

ABSTRACT

Controlling ferroelectric switching in Mg doped lithium niobate (Mg:LN) is of fundamental importance for optical device and domain wall electronics applications that require precise domain patterns. Stable ferroelectric switching has previously been observed in undoped LN layers above proton exchanged (PE) phases that exhibit reduced polarization, whereas PE layers have been found to inhibit lateral domain growth. Here, Mg doping, which is known to significantly alter ferroelectric switching properties including coercive field and switching currents, is shown to inhibit domain nucleation and stability in Mg:LN above buried PE phases which allows for precise ferroelectric patterning via domain growth control. Furthermore, piezoresponse force microscopy and switching spectroscopy reveal that the voltage at which polarization switches from the "up" to the "down" state increases with increasing thickness in pure Mg:LN whereas the voltage required for stable back switching to the original "up" state does not exhibit this thickness dependence, which is consistent with the presence of an internal frozen defect field. The inhibition of domain nucleation above PE interfaces, observed in this study, is a phenomenon that occurs in Mg:LN but not undoped samples and is mainly ascribed to a remaining frozen polarization in the PE phase that opposes polarization reversal. This reduced frozen depolarization field in the PE phase also influences the depolarization field of the Mg:LN layer above due to the presence of uncompensated polarization charge at the PE-Mg:LN boundary. These alterations in internal electric fields within the sample cause long-range lattice distortions in Mg:LN via electromechanical coupling that were corroborated with complimentary Raman measurements.

I. INTRODUCTION

The development of a reliable periodic poling technology for congruent lithium niobate (LN) has led to the efficient exploitation of its large optical nonlinearity and spontaneous polarization in a variety of applications, ranging from optical telecommunications and frequency conversion[1,2] to ferroelectric lithography[3–5] and artificial photosynthesis.[6] However, optical and ferroelectric properties can be improved by high concentration Mg doping, which has gained significant interest for applications in optics, especially due to the high resistance to photorefraction of Mg doped LN (Mg:LN) crystals.[7,8] Combined with a lower coercive field compared to undoped crystals, periodically poled Mg:LN is therefore a promising material for quasi phase matched devices[9–11] and applications based on domain wall electronics where the locally enhanced photoconductivity at the domain boundaries[12,13] can be exploited. With these applications in mind, domain reversal induced by an externally applied field,[10,11,14–16] illumination[17] or temperature variation[18] has been studied macroscopically and on the micro- or nanoscale to gain control over the switching process. The achievement of precise domain patterning for ferroelectric gratings is particularly crucial for the aforementioned applications, which remains a challenge at small scales due to sideways growth of domains and coalescence.[19,20] In undoped LN, proton exchange, a chemical modification of the crystal lattice by introduction of protons and depletion of Li ions that leads to loss of ferroelectricity, has been demonstrated to (i) inhibit switching in the LN layer beneath the PE phase and (ii) limit lateral domain expansion if the proton exchanged (PE) phases are located at the surface where electric field poling is initiated.[19,20] However, if the PE phase is located beneath a layer of undoped LN, stable domain switching is not suppressed.[21] The proton exchange process is commonly used in optics for the fabrication of waveguides.[22–25] Although little knowledge exists about the effect of PE phases on the surrounding ferroelectric crystal matrix, this technique allows for precise local

structural modifications and is therefore an interesting option for domain growth control. PE assisted domain engineering has not been investigated yet for doped Mg:LN crystals and cannot be inferred from results obtained on undoped LN. Mg doping is known to change ferroelectric properties with respect to the well-understood behavior of undoped LN, most notably the onset of diode-like conduction after polarization switching and much longer (almost 3 orders of magnitude) stabilization times for freshly poled domains.[11,26,27] In order to gain further control over domain engineering in Mg:LN, the aims of this work are to (i) demonstrate a method to tailor micro- and nanoscale domain patterning through local inhibition of domain growth in Mg:LN, (ii) provide further insight into switching kinetics in Mg:LN and (iii) explore the structural impact of the introduction of PE phases on the surrounding Mg:LN crystal matrix, which affects ferroelectric behavior. Therefore, switching studies using piezoresponse force microscopy[28,29] (PFM) and switching spectroscopy PFM[30] (SSPFM) were performed on a wedge-shaped Mg:LN substrate exhibiting PE phases at the bottom surface, which allows to assess ferroelectric properties in dependence of sample composition and thickness. In a next step, complementary Raman spectroscopy[31] was used to detect the PE induced changes and effects on the surrounding crystal matrix and related to ferroelectric properties.

II. MATERIALS AND METHODS

A z-cut 5 mol% MgO doped congruent LN substrate having a thickness of 500 µm (Roditi Ltd.) was periodically proton exchanged along the crystallographic x-axis by exposing the -z surface through periodic mask openings to benzoic acid at 210°C for 48 h, as described elsewhere.[19,32] The maximum depth of these PE channels into the Mg:LN substrate is 5.87 µm as measured with an optical prism coupling technique.[33] Apart from the periodic PE

channels, proton exchange also took place at isolated locations within the alternating LN stripes due to fine openings in the mask that allowed for shallow localized PE islands, which are visible in light microscope images (Figure 1(a)). Chemo-mechanical wedge polishing (angle ≈14°) with an alkaline sub-micron colloidal silica solution (SF1 Polishing Solution, Logitech) was performed on the +z surface to obtain a cross section of the PE areas while preserving the polar orientation in the vertical direction (Figure 1(b)). The obtained wedge shape allows for sample thickness and composition dependent experimental studies. A ≈100 nm thick gold layer was deposited on the -z surface through thermal evaporation in vacuum as a bottom electrode and connected to a copper circuit board with silver paint.

Sample topography was imaged with contact mode atomic force microscopy (AFM) (MFP-3D, Asylum Research). The electromechanical behavior of different sample areas was measured using PFM by applying an AC voltage (5 V amplitude, 20 kHz) to a conductive tip (PPP-EFM Nanosensors, 2.8 N/m, 75 kHz) and recording the deformation of the surface due to the converse piezoelectric effect.[28,29] In order to obtain the amplitude of the voltage induced oscillations and local polarization direction, the cantilever movement is demodulated into PFM amplitude and phase signals using an external lock-in amplifier (HF2LI, Zurich Instruments) equipped with an adder for the simultaneous application of AC and DC voltages. A high voltage amplifier (FLC Electronics, F10A) was used to amplify AC and DC voltages for switching experiments.

The local ferroelectric properties of a 20 × 20 μm^2 area of the sample were investigated using SSPFM[30] by applying a triangular waveform consisting of DC square pulses in a grid of 20 × 20 points and collecting the hysteresis loops extracted from the PFM data recorded after each pulse. A switching distance of 1 µm was chosen to ensure resultant domains are non-

coalescent under ambient conditions. Switching and data acquisition started at the bottom left corner and proceeded continuously to the top. The SSPFM waveform consisted of three parts during which the polarization orientation was switched by applying square pulses of 50 ms duration (ON) followed by a 50 ms pause (OFF): ON pulses increased from 0 to +70 V in steps of 28 V to switch the polarization orientation from "up" to "down" and then decreased stepwise to 0 V again (part 1); subsequently, the polarization was reversed to its "up" state again by applying the same waveform of negative polarity (part 2); switching to the "down" state was repeated to obtain a domain pattern visible in subsequent PFM scans and to assess long term domain stability (part 3). The data for hysteresis loops and the voltage at which full stable polarization reversal occurs from "up" to "down" (V_{down}) and "down" to "up" (V_{up}) were extracted from PFM amplitude and phase signals acquired during parts 1 and 2 of the SSPFM waveform.

Raman spectra from 100 to 1100 cm^{-1} were measured with a confocal Raman spectrometer (Renishaw 1000) by focusing a laser (λ = 532 nm) on the sample surface with a 50x objective and collecting the scattering through the same objective in $\bar{Z}$(YY)Z backscattering geometry. Raman maps were acquired at the wedge edge of Mg doped samples across PE and Mg:LN areas with a step size of 1 μm (in x- and y directions) and an integration time of 10 s. The spectrophotometer was calibrated using a characteristic silicon line at 520.5 cm^{-1}. All spectra were normalized with respect to the highest peak and the peaks were fitted assuming a mixture of Lorentzian and Gaussian shapes, after a baseline correction. Peak fitting parameters included peak intensity, position, and width at half height for each spectrum, from which image maps were constructed using interpolation of neighboring pixels.

III. RESULTS AND DISCUSSION

The topography appears homogeneous within the investigated sample areas despite their varying composition and crystal structure (Figure 2(a, b)) while PFM amplitude and phase images show contrast between Mg:LN and the exposed PE area where piezoresponse is reduced (Figure 2(c, d)), consistent with prior reports.[34] From the known depth and wedge angle of the PE channel, a thickness range of 4.34 µm to 9.18 µm within the depicted scan size can be calculated. After applying SSPFM pulses, domain stability is assessed in subsequent PFM images. From the acquired PFM signal recorded in between the applied DC pulses during SSPFM (OFF state), hysteresis loops can be extracted for each grid point, revealing differences in ferroelectric properties due to sample composition and thickness. Unlike PFM images, hysteresis loops allow the onsets of switching as well as full but unstable polarization reversal to be tracked as the signal is recorded immediately after the voltage pulses during the subsequent 50 ms. While electrical AFM modes are valuable tools to investigate ferroelectric behavior, Raman spectroscopy was employed in order to elucidate underlying effects of the observed switching properties such as the structural impact of PE on the surrounding Mg:LN.

The experimental observations yield the following findings that will be discussed in detail in the subsections below: (i) buried PE areas inhibit stable domain switching in ferroelectric Mg:LN layers, (ii) the voltages at which stable switching occurs is thickness dependent only for forward switching, and (iii) the introduction of PE phases leads to long-range distortions in the embedding Mg:LN matrix that correspond to changes in depolarization fields in PE and Mg:LN, which affect ferroelectric behavior.

Switching inhibition in Mg:LN above PE areas

After applying SSPFM to each grid point, a pattern of stably switched domains is visible in PFM images (Figure 3(a, b)). It is apparent that stable polarization reversal in Mg:LN is impeded by buried PE layers regardless of the thickness of the Mg:LN above. The obstructed switching on the left side of the amplitude and phase images depicted in Figure 3(a, b) is due to an adjacent PE area outside of the scanning range. Empty spots in the domain pattern in the Mg:LN stripe mark the position of buried shallow PE islands at the -z surface that are otherwise invisible to surface imaging microscopy techniques like PFM. The reduced thickness of these islands compared to the periodic deep PE channels can be inferred from the fact that although present throughout all Mg:LN areas in the whole sample, none are exposed by wedge polishing, indicating a depth of < 2.18 µm.

Inhibition of domain switching above PE is a phenomenon that was observed in Mg:LN only. A control experiment on a similar but undoped LN sample of equal composition and polarization at a matching sample thickness of 4.06 to 8.89 µm showed stably switched domains in the whole grid, which was taken at a switching distance of 2 µm that also allows for single, non-coalescent domains (Figure 3(c, d)).

In order to understand inhibition of switching above PE, internal electric fields within the sample have to be considered as well as differences between undoped and Mg doped LN. PE leads to deterioration of ferroelectricity, which results in a lower, yet present, polarization[34] that cannot be switched. The resulting frozen PE depolarization field counteracts switching as it makes the initial polarization state energetically favorable and increases the energy barrier for polarization reversal. This effect has been commonly derived thermodynamically in free energy models and is also employed to explain asymmetries in hysteresis loops due to

internal defect fields that arise from frozen defect clusters.[35,36] In addition, the depolarization field in the Mg:LN above PE is increased due to uncompensated bound charges at the PE interface compared to Mg:LN terminated by metal electrodes.[37] It has been shown previously that in LN a 83% decrease in polarization occurs in the PE phase, while in Mg:LN only a reduction of 68% is present.[34] Therefore, the counteracting frozen PE depolarization field is higher in Mg doped samples, which explains the observed differences in domain stability above PE layers between LN and Mg:LN.

Thus, from the SSPFM data extracted PFM phase and amplitude loops show that the thickness of the buried PE layer influences domain evolution (Figure 4(a, b)). In and above the exposed PE area there is no significant change in PFM phase at positive and only small variations at negative voltages. Independent of the thickness of the Mg:LN layer (up to 3.31 µm) above the PE channel, there was no onset of switching observed, in agreement with the behavior in the exposed PE region. However, adjacent to the exposed PE area where the underlying PE layer is thinner and exhibits a strong curvature, unstable phase changes were measured. Full switching from “up” to “down” and “down” to “up” polarization states can also occur at Mg:LN areas with shallow PE islands underneath, implying that both the thickness and composition of the PE layer play a role in domain formation. However, the fact that the domains are not visible in PFM amplitude and phase images leads to the conclusion that these domains are not stable. In contrast, at adjacent switching positions in pure Mg:LN, stable domain switching is permitted and shows thickness dependent domain kinetics that can be utilized for further control of domain growth.

Thickness dependence of ferroelectric switching

In the absence of buried PE layers, stable switching within part 1 and 2 of the SSPFM cycle is observed up to 8.67 µm thickness. Here, the thickness of the Mg:LN layer mainly determines the voltage at which stable switching to "down" polarization states occurs V_{down} (Figure 4(c, d)). Switching voltages were extracted only for stably switched domains from phase hysteresis loops with V_{down}, exhibiting a pronounced thickness dependence, whereas the values for V_{up}, show a much weaker effect (Figure 5(a)). The difference in these switching voltages, ΔV_S, is therefore also thickness dependent. Considering the simplified relation $V \sim E \cdot t$ with the voltage, V, the electric field, E, and the Mg:LN thickness, t, differences in the slopes of switching voltages can be ascribed to a change in E. However, the asymmetry and different behavior of switching voltages for "up" and "down" polarization states can be ascribed to frozen Nb antisites - Li vacancy clusters, which are common in LN and the origin of frozen defect fields that favor the initial polarization orientation.[38,39] The strength of this defect field is estimated from the asymmetry in E_{up} and E_{down} as depicted in Figure 5(b) to be 2.34 ± 0.47 kV/mm and shows no thickness dependence. While in undoped congruent LN internal defect fields of this order of magnitude are expected, fields of only ≈ 0.5 kV/mm are reported for Mg:LN as high concentration doping leads to a reduction in vacancies.[15,40–42] However, the values from literature were obtained macroscopically from coercive fields on non PE samples, whereas here the internal defect field is inferred from the stable switching voltages as measured with a nanosized probe upon switching of a single domain in periodically PE Mg:LN. Therefore, also contributions to the measured internal electric fields by PE induced long-range distortions are likely and will be further investigated in the following section.

Long-range distortions imposed by PE

From the 4 A and 9 E Raman active transversal and longitudinal phonons in LN, only 4 A(LO) that describe longitudinal ion displacement along the z-axis (around 270 cm^{-1}, 330 cm^{-1},430 cm^{-1}, and 869 cm^{-1}), and 7 non stoichiometric E(TO) bands that represent transversal oscillations in the x- or y- direction (around 149 cm^{-1}, 234 cm^{-1}, 258 cm^{-1}, 326 cm^{-1}, 361 cm^{-1}, 429 cm^{-1}, and 577 cm^{-1}), are permitted in the chosen configuration of $\bar{Z}(YY)Z$ and are visible in the spectra (Figure 6(a), red line).[43–46] Incorporation of Mg^{2+} ions into the crystal leads to changes in parameters (intensity, position, width) of existing peaks especially if the sites of involved oscillations are occupied by the dopants.[40,45,47] Furthermore, bands that would usually not be permitted for symmetry reasons appear and are ascribed to photorefraction[45,48,49] and defect induced symmetry breaking,[50] which explains the $A(TO_4)$ band visible around 625 cm^{-1}. Also proton exchange leads to significant alterations of the spectra due to lattice disorder.[51–54] The original lines of the substrate are still present, but broadened and changed in intensity, Figure 6(a). A characteristic phonon frequency 680 cm^{-1} originated in distortion of Nb^{5+} octahedra towards non polar states[53–55] exhibits a high intensity in exposed PE areas. Only the edge of a PE band[54] located at 69 cm^{-1} is visible within the measured spectral range. A new peak at 960 cm^{-1} appears and is assigned to OH^- librational bands that are strongly dependent on the proton exchange phase.[55,56] Having assigned spectral characteristics it is possible to monitor the influence of PE across the sample as well as strains indicated by peak broadening and position shift.[31] In Raman spectra (Figure 6(a)) extracted at different positions on the sample (red: 20 µm thick Mg:LN; blue: exposed PE area; green: 14.1 µm thick Mg:LN above 5.9 µm PE, as also approximately indicated by colored crosses in the intensity map, Figure 6(b)), this peak is unexpectedly visible as a shoulder on the Mg:LN stripe and is even more pronounced above the PE channel (spectral area of interest shaded in light blue). The intensity map of the 680 cm^{-1} peak

exhibits high signals from the exposed PE area and from PE covered by a thin layer of Mg:LN. Furthermore, that band is enhanced at Mg:LN areas above shallow PE islands compared to the surrounding Mg:LN (Figure 6(b)). In addition, characteristic peaks for pure LN and Mg:LN exhibit reduction in intensity, peak broadening, and shifts in peak positions. As an example, maps for each peak parameter of the 149 cm^{-1} $E(TO_1)$ band (spectral area highlighted in light yellow in Figure 6(a)), are extracted and shown in Figure 6(c). This peak represent out of phase displacement of Nb^{5+} and O^{2-} ions along the crystallographic y-axis,[57] and exhibits spectral changes that vary within the exposed PE areas and show less prominent changes with increasing Mg:LN thickness. As the oscillation of ions can be affected by electric fields and corresponding electromechanical strains in the crystal lattice, the observed composition dependent Raman contrast supports the anticipated change in Mg:LN depolarization fields due to uncompensated polarization charges at the PE interface.[58] In addition, mechanically imposed strains might contribute to lattice distortions as Mg:LN and LN undergo structural changes through unit cell expansion upon proton exchange.[59,60] It is therefore evident that the introduction of PE phases does not only modify the crystal lattice locally but also leads to long range distortions of the embedding Mg:LN matrix.

IV. CONCLUSIONS

Here, it is shown that nanoscale domain patterns for, e.g., ferroelectric Mg:LN gratings in optical and electronic devices can be obtained by domain growth control via PE phases and sample thickness. Switching spectroscopy and subsequent PFM imaging of a periodically PE Mg:LN wedge shaped sample having +z polar orientation revealed significant differences in ferroelectric behavior between pure Mg:LN in direct contact with the metal bottom electrode and Mg:LN above PE phases. In pure Mg:LN, stable switching was observed. Furthermore, a

linear thickness dependence of the voltage required for stable polarization switching from "up" to "down" state, V_{down}, was measured while the voltage for polarization reversal to the original state, V_{up}, remained approximately constant, which can be ascribed to large frozen defect fields.[39,61] In Mg:LN above buried PE phases, stable polarization reversal is prevented, which is in contrast to observations in undoped LN. This effect is ascribed to the strong remaining frozen polarization in the PE phase of Mg:LN that counteracts switching and is greatly reduced in undoped LN. Onsets of polarization reversal were observed in some Mg:LN areas above shallow PE islands and edges of the PE channel while domain nucleation was completely inhibited in Mg:LN directly above the thickest part of the PE channel. Due to uncompensated polarization charges at the Mg:LN boundaries, the depolarization field is changed compared to pure Mg:LN, which via electromechanical coupling and in combination with mechanically imposed strain, leads to long-range distortions that were corroborated by Raman spectroscopy. Apart from domain engineering, the wide range of these distortions in Mg:LN areas above PE, might also have an impact on optical applications via the elasto-optic effect.

ACKNOWLEDGEMENTS

This research was funded by the European Commission within FP7 Marie Curie Initial Training Network "Nanomotion" (grant agreement nº 290158). The AFM used for this work was funded by Science Foundation Ireland (SFI07/IN1/B931). Raman measurements were conducted at the Center for Nanophase Materials Sciences which is a DOE Office of Science User Facility (CNMS2015-139). The authors would also like to thank Ivan Kravchenko for depositing the gold bottom electrode at CNMS. ALK acknowledges the CICECO-Aveiro Institute of Materials (Ref. FCT UID/CTM/50011/2013), financed by national

funds through the FCT/MEC and when applicable co-financed by FEDER under the PT2020 Partnership Agreement. KG gratefully acknowledges support from the Swedish Research Council through a Senior Fellowship (622-2010-526) and research grant no. 621-2014-5407.

FIGURES

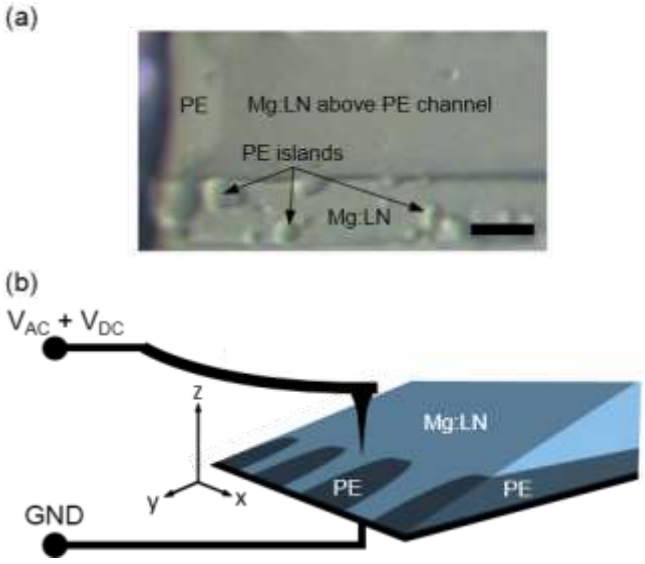

FIG. 1. (a) Light microscope image of sample showing regions of different composition (scale bar 10 μm) and (b) scheme of sample and experimental setup for PFM and SSPFM.

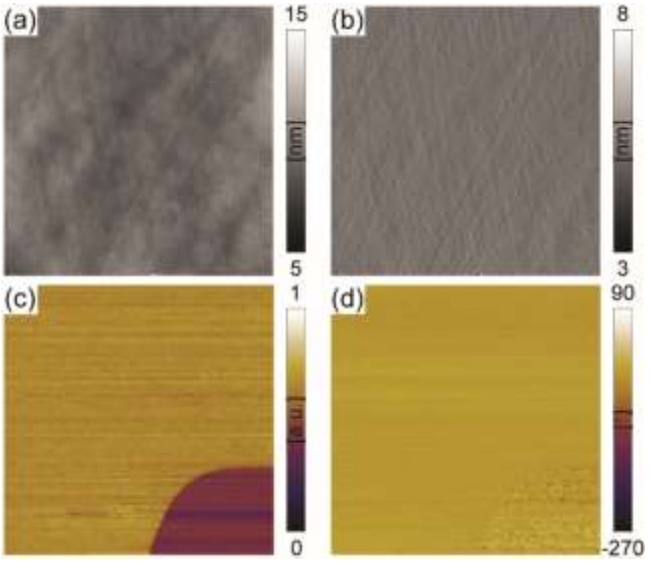

FIG. 2. AFM images of (a) height, (b) deflection, (c) PFM amplitude, and (d) PFM phase before application of SSPFM waveform on PE Mg:LN (scan size 20×20 μm^2, offset flattening applied).

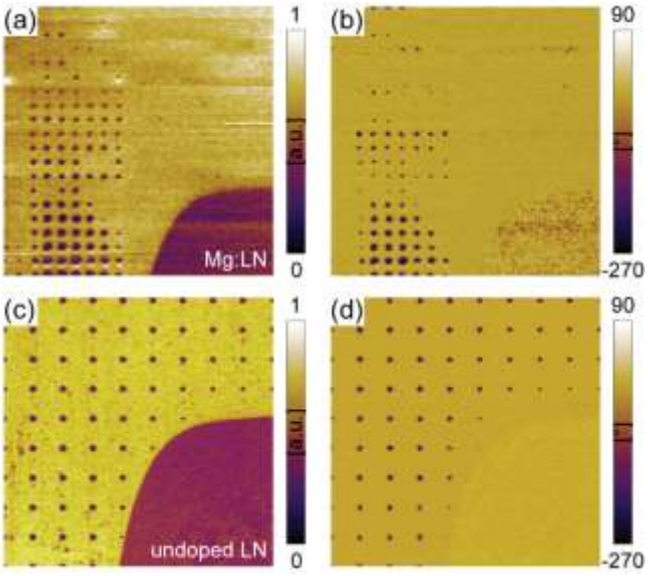

FIG. 3. PFM (a, c) amplitude (normalized) and (b, d) phase images recorded after application of the SSPFM waveform over the whole scan size on (a, b) Mg:LN (switching distance 1 μm) and (c, d) undoped LN (switching distance 2 μm) (scan sizes 20×20 μm^2, offset flattening applied to a and b).

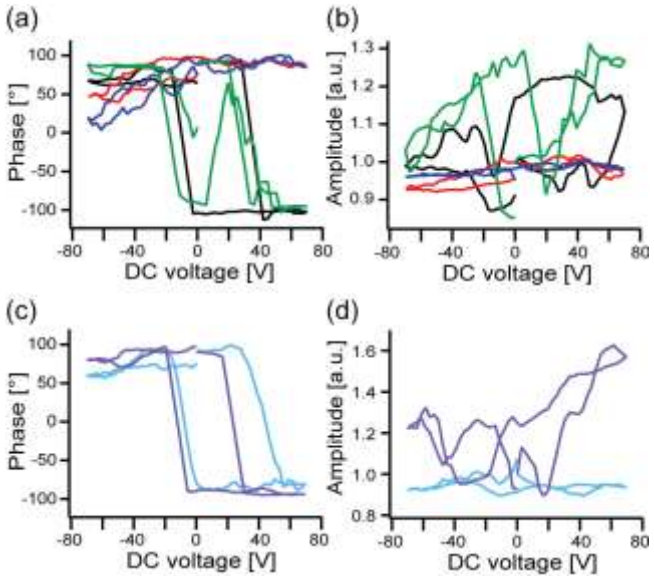

FIG. 4. Representative SSPFM hysteresis loops (moving average smoothing filter applied) measured on (a, b) areas with PE layers (blue: in exposed PE channel area, red: above PE channel, green: beside exposed PE channel area, black: above shallow PE island) and (c, d) Mg:LN (purple: at 4.34 μm thickness, light blue: at 8.16 μm).

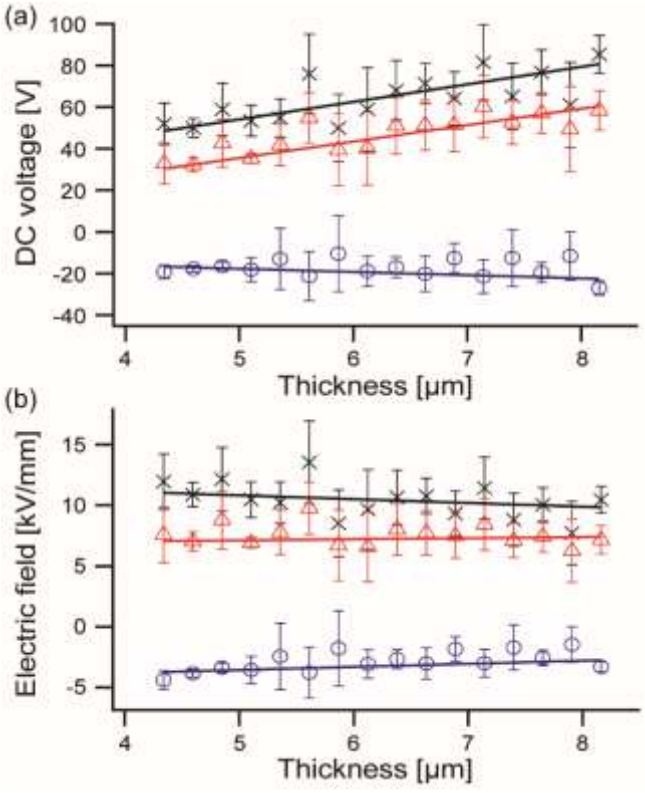

FIG. 5. (a) Switching voltages and (b) corresponding electric fields of stable Mg:LN domains as a function of sample thickness (red Δ: V_{down} /E_{down}, blue ○: V_{up} /E_{up}, black ×: $\Delta V_S = V_{down} - V_{up}$ / $\Delta E_S = E_{down} - E_{up}$), solid lines are linear fits of data points, weighted by error bars.

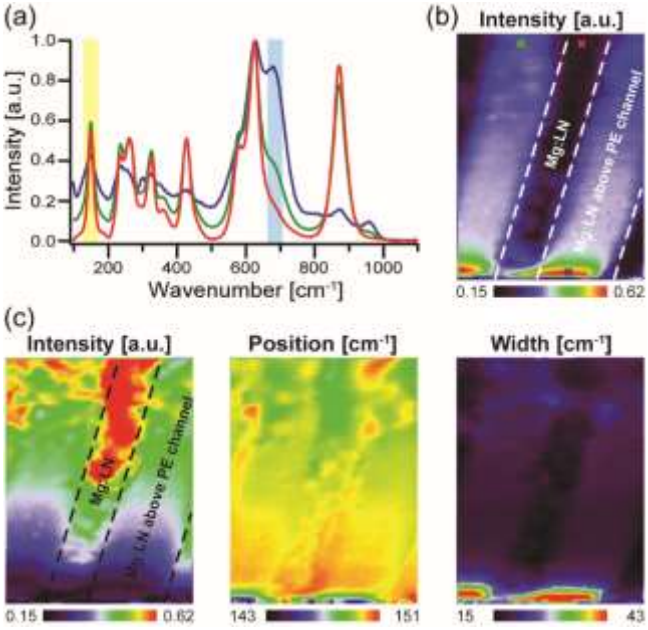

FIG. 6. (a) Raman spectra extracted from three different positions on the sample surface (red: 20 μm thick Mg:LN, blue: exposed PE area, green: 14.1 μm thick Mg:LN above 5.9 μm PE) approximately indicated by colored crosses in (b) the Raman intensity map of the 680 cm^{-1} peak (highlighted in blue in spectra graph). (c) Raman intensity, position, and width maps of the 149 cm^{-1} peak (highlighted in yellow in spectra graph) (map image sizes 54×71 μm^2; exposed PE area at bottom).

REFERENCES

[1] C. Langrock, S. Member, and A.E. Willner, J. Light. Technol. **24**, 2579 (2006).

[2] S. Liu, K.J. Lee, F. Parmigiani, J. Kakande, K. Gallo, P. Petropoulos, and D.J. Richardson, Opt. Express **19**, 11705 (2011).

[3] J.N. Hanson, B.J. Rodriguez, R.J. Nemanich, and a Gruverman, Nanotechnology **17**, 4946 (2006).

[4] L. Balobaid, N. Craig Carville, M. Manzo, L. Collins, K. Gallo, and B.J. Rodriguez, Appl. Phys. Lett. **103**, 182904 (2013).

[5] N.C. Carville, M. Manzo, S. Damm, M. Castiella, L. Collins, D. Denning, S.A.L. Weber, K. Gallo, J.H. Rice, and B.J. Rodriguez, ACS Nano **6**, 7373 (2012).

[6] M. Stock and S. Dunn, IEEE Trans. Ultrason. Ferroelectr. Freq. Control **58**, 1988 (2011).

[7] D.A. Bryan, R. Gerson, and H.E. Tomaschke, Appl. Phys. Lett. **44**, 847 (1984).

[8] K. Sweeney, L. Halliburton, D. Bryan, R. Rice, R. Gerson, and H. Tomaschke, J. Appl. Phys. **57**, 1036 (1985).

[9] Y. Chen, W. Yan, J. Guo, S. Chen, G. Zhang, and Z. Xia, Appl. Phys. Lett. **87**, 212904 (2005).

[10] K. Nakamura, J. Kurz, K. Parameswaran, and M.M. Fejer, J. Appl. Phys. **91**, 4528 (2002).

[11] K. Mizuuchi, A. Morikawa, T. Sugita, and K. Yamamoto, J. Appl. Phys. **96**, 6585 (2004).

[12] M. Schröder, A. Haußmann, A. Thiessen, E. Soergel, T. Woike, and L.M. Eng, Adv. Funct. Mater. **22**, 3936 (2012).

[13] S.M. Neumayer, M. Manzo, A.L. Kholkin, K. Gallo, and B. Rodriguez, Unpublished (n.d.).

[14] M.L. Hu, L.J. Hu, and J.Y. Chang, Jpn. J. Appl. Phys. **42**, 7414 (2003).

[15] J.H. Yao, Y.H. Chen, B.X. Yan, H.L. Deng, Y.F. Kong, S.L. Chen, J.J. Xu, and G.Y. Zhang, Phys. B Condens. Matter **352**, 294 (2004).

[16] V.Y. Shur, A.V. Ievlev, E.V. Nikolaeva, E.I. Shishkin, and M.M. Neradovskiy, J. Appl. Phys. **110**, 052017 (2011).

[17] C.E. Valdivia, C.L. Sones, J.G. Scott, S. Mailis, R.W. Eason, D.A. Scrymgeour, V. Gopalan, T. Jungk, E. Soergel, and I. Clark, Appl. Phys. Lett. **86**, 022906 (2005).

[18] V.Y. Shur, E.A. Mingaliev, V.A. Lebedev, D.K. Kuznetsov, and D. V. Fursov, J. Appl. Phys. **113**, 187211 (2013).

[19] M. Manzo, F. Laurell, V. Pasiskevicius, and K. Gallo, Opt. Mater. Express **1**, 365 (2011).

[20] M. Manzo, F. Laurell, V. Pasiskevicius, and K. Gallo, Appl. Phys. Lett. **98**, 122910 (2011).

[21] M.A. Dolbilov, V.Y. Shur, E.I. Shishkin, M.F. Sarmanova, E.V. Nikolaeva, S. Tascu, P. Baldi, and M.P. de Micheli, Ferroelectrics **374**, 14 (2008).

[22] J.L. Jackel, Electron. Lett. **21**, 509 (1985).

[23] M. Digonnet, M. Fejer, and R. Byer, Opt. Lett. **10**, 235 (1985).

[24] J.L. Jackel, C.E. Rice, and J.J. Veselka, Electron. Lett. **19**, 387 (1983).

[25] S. Klauer, M. Woehlecke, and S. Kapphan, Phys. Rev. B **45**, 2786 (1992).

[26] A. Kuroda, S. Kurimura, and Y. Uesu, Appl. Phys. Lett. **69**, 1565 (1996).

[27] V.Y. Shur, I.S. Baturin, A.R. Akhmatkhanov, D.S. Chezganov, and A.A. Esin, Appl. Phys. Lett. **103**, 102905 (2013).

[28] S. V Kalinin, A. Rar, and S. Jesse, IEEE Trans. Ultrason. Ferroelectr. Freq. Control **53**, 2226 (2006).

[29] N. Balke, I. Bdikin, S. V. Kalinin, and A.L. Kholkin, J. Am. Ceram. Soc. **92**, 1629 (2009).

[30] S. Jesse, A.P. Baddorf, and S.V. Kalinin, Appl. Phys. Lett. **88**, 062908 (2006).

[31] G. Gouadec and P. Colomban, Prog. Cryst. Growth Charact. Mater. **53**, 1 (2007).

[32] M. Manzo, F. Laurell, V. Pasiskevicius, and K. Gallo, Appl. Phys. Lett. **98**, 6 (2011).

[33] K. Chiang, J. Light. Technol. **3**, 385 (1985).

[34] M. Manzo, D. Denning, B.J. Rodriguez, and K. Gallo, J. Appl. Phys. **116**, 066815 (2014).

[35] A. Morozovska, S. Kalinin, E. Eliseev, V. Gopalan, and S. Svechnikov, Phys. Rev. B **78**, 125407 (2008).

[36] T. Volk and M. Wöhlecke, *Lithium Niobate - Defects, Photorefraction and Ferroelectric Switching* (2008).

[37] M.B. Okatan, J. V. Mantese, and S.P. Alpay, Phys. Rev. B - Condens. Matter Mater. Phys. **79**, 174113 (2009).

[38] V. Gopalan and M.C. Gupta, Ferroelectrics **198**, 49 (1997).

[39] V. Gopalan, V. Dierolf, and D.A. Scrymgeour, Annu. Rev. Mater. Res. **37**, 449 (2007).

[40] R. Mouras, M.D. Fontana, P. Bourson, and A. V. Postnikov, J. Phys. Condens. Matter **12**, 5053 (2000).

[41] A. V. Yatsenko, S. V. Yevdokimov, D.Y. Sugak, and I.M. Solskii, Acta Phys. Pol. A **117**, 166 (2010).

[42] V. Gopalan, T.E. Mitchell, Y. Furukawa, and K. Kitamura, Appl. Phys. Lett. **72**, 1981 (1998).

[43] V. Caciuc, A. Postnikov, and G. Borstel, Phys. Rev. B **61**, 8806 (2000).

[44] A. Ridah, P. Bourson, M.D. Fontana, and G. Malovichko, J. Phys. Condens. Matter 9687 (1999).

[45] N. V. Sidorov, A.A. Gabain, A.A. Yanichev, I.N. Efremov, I. V. Biryukova, and M.N. Palatnikov, Opt. Spectrosc. **118**, 269 (2015).

[46] S. Margueron, a. Bartasyte, a. M. Glazer, E. Simon, J. Hlinka, I. Gregora, and J. Gleize, J. Appl. Phys. **111**, (2012).

[47] K. Lengyel, L. Kovàcs, À. Pèter, K. Polgàr, G. Corradi, and P. Bourson, Phys. Status Solidi Curr. Top. Solid State Phys. **4**, 847 (2007).

[48] R. Mouras, S.M. Kostritskii, P. Bourson, M. Aillerie, and M.D. Fontana, Opt. Mater. (Amst). **18**, 127 (2001).

[49] N. V. Sidorov, P.G. Chufyrev, M.N. Palatnikov, N.N. Mel'nik, and V.T. Kalinnikov, Inorg. Mater. **41**, 210 (2005).

[50] E. Giulotto, R. Decontardi, F. Rossella, and V. Bermudez, in *Photorefractive Eff. Mater. Devices* (2003), p. 90.

[51] G.R. Paz-Pujalt and D.D. Tuschel, Appl. Phys. Lett. **62**, 3411 (1993).

[52] I. Savatinova, S. Tonchev, E. Liarokapis, M.N. Armenise, and M. Armenise, Appl. Phys. A Mater. Sci. Process. **68**, 483 (1999).

[53] M. Kuneva, S. Tonchev, E. Thatsi, and D. Lampakis, J. Optoelectron. Adv. Mater. **7**, 549 (2005).

[54] M. Kuneva and S. Tonchev, Bulg. Chem. Commun. **43**, 276 (2011).

[55] S.M. Kostritskii, Y.N. Korkishko, V.A. Fedorov, D.B. Maring, R.F. Tavlykaev, and R. V. Ramaswamy, J. Appl. Phys. **91**, 930 (2002).

[56] A. Gröne and S. Kapphan, J. Phys. Condens. Matter **7**, 3051 (1995).

[57] P.S. Zelenovskiy, M.D. Fontana, V.Y. Shur, P. Bourson, and D.K. Kuznetsov, Appl. Phys. A Mater. Sci. Process. **99**, 741 (2010).

[58] G. Stone, B. Knorr, V. Gopalan, and V. Dierolf, Phys. Rev. B - Condens. Matter Mater. Phys. **84**, 1 (2011).

[59] S. Chen, P. Baldi, M.P. De Micheli, D.B. Ostrowsky, A. Leycuras, G. Tartarini, and P. Bassi, J. Light. Technol. **12**, 862 (1994).

[60] Y.N. Korkishko, V.A. Fedorov, S.M. Kostritskii, E.I. Maslennikov, M. V. Frolova, A.N. Alkaev, C. Sada, N. Argiolas, and M. Bazzan, J. Appl. Phys. **94**, 1163 (2003).

[61] M. Molotskii, J. Appl. Phys. **93**, 6234 (2003).

(a)

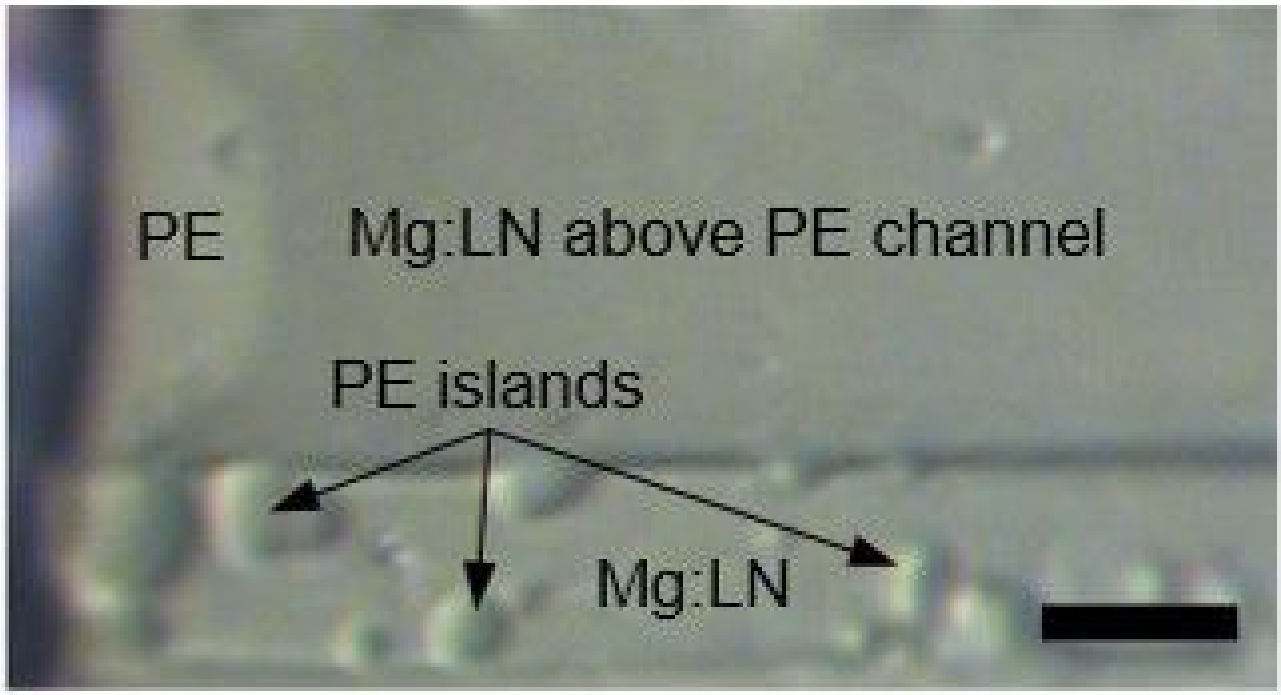
PE
Mg:LN above PE channel
PE islands
Mg:LN

(b)

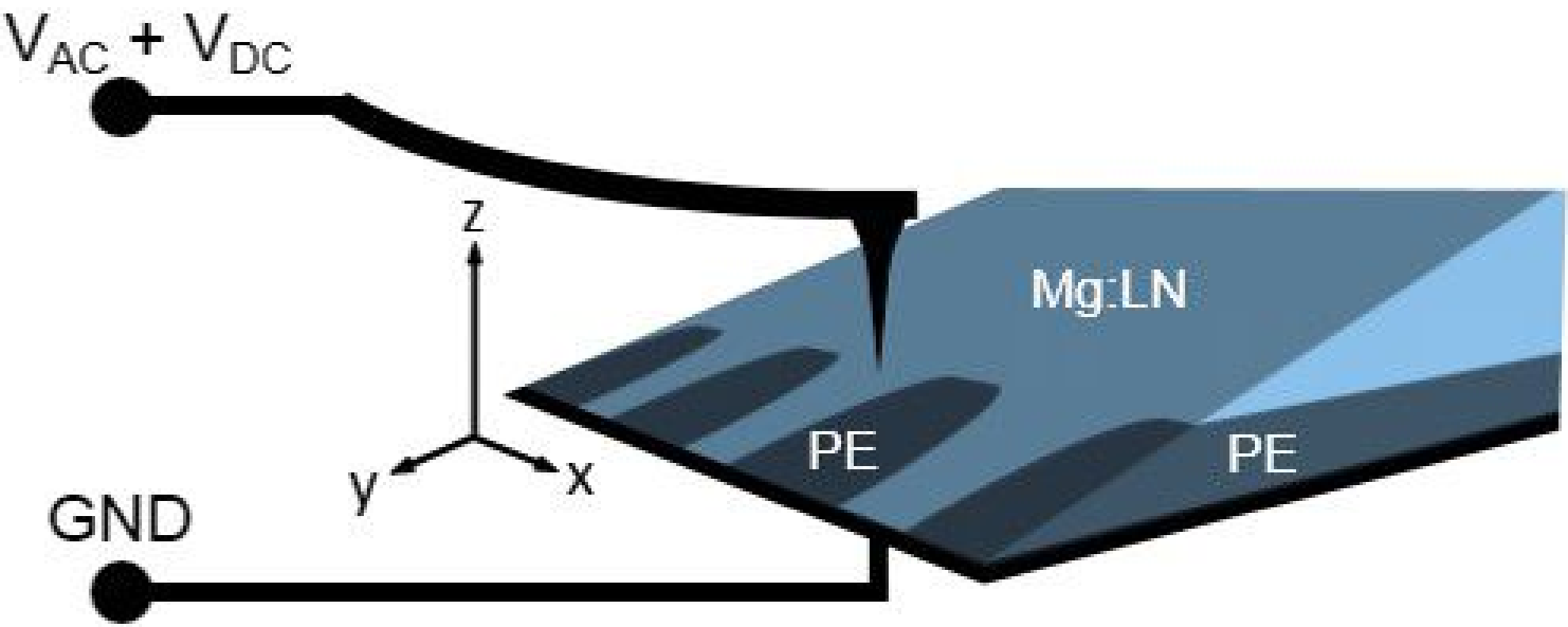
$V_{AC} + V_{DC}$
z
y
x
Mg:LN
PE
PE
GND

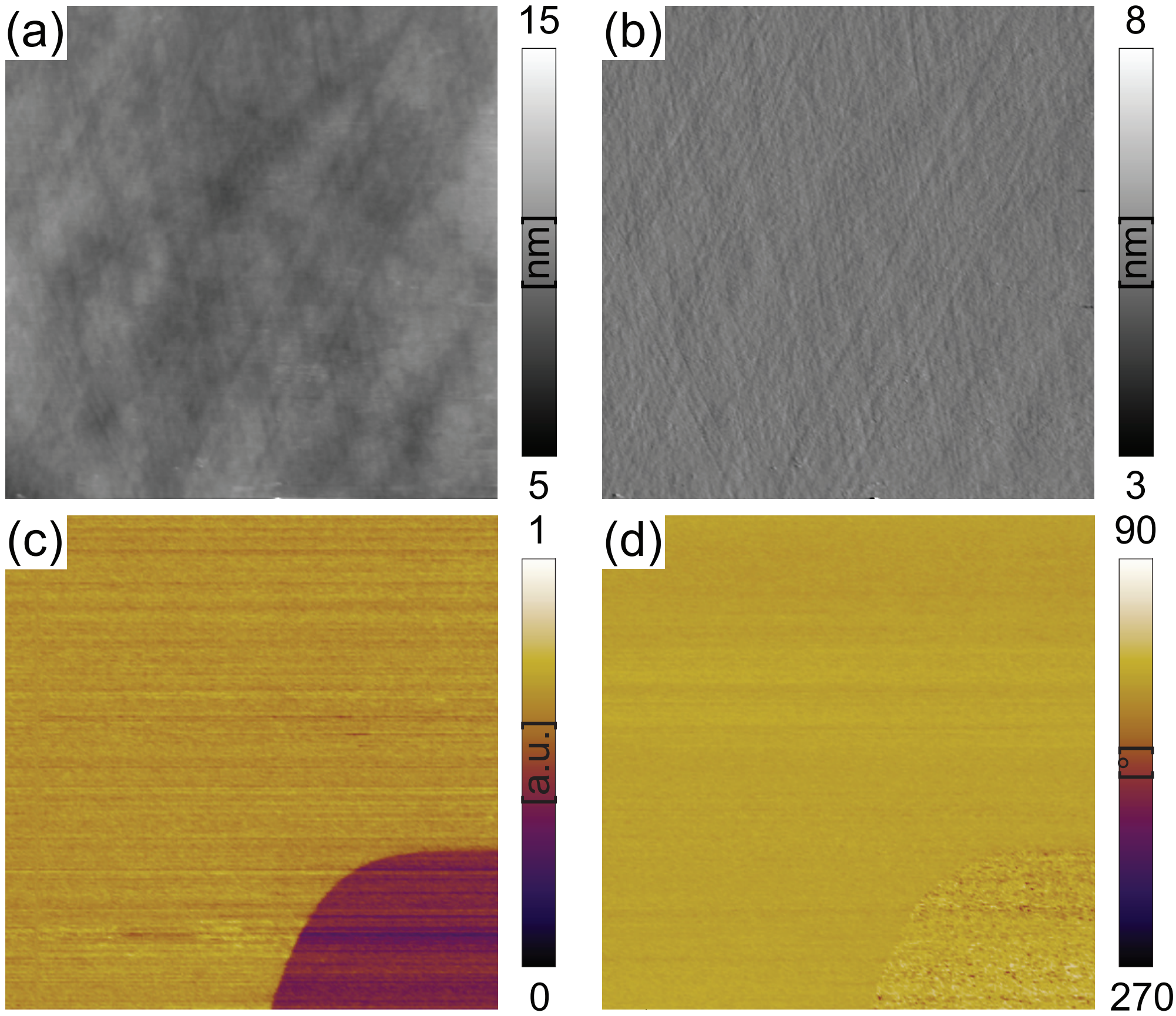
(a)
15
[nm]
5
(b)
8
[nm]
3
(c)
1
[a.u.]
0
(d)
90
[°]
270

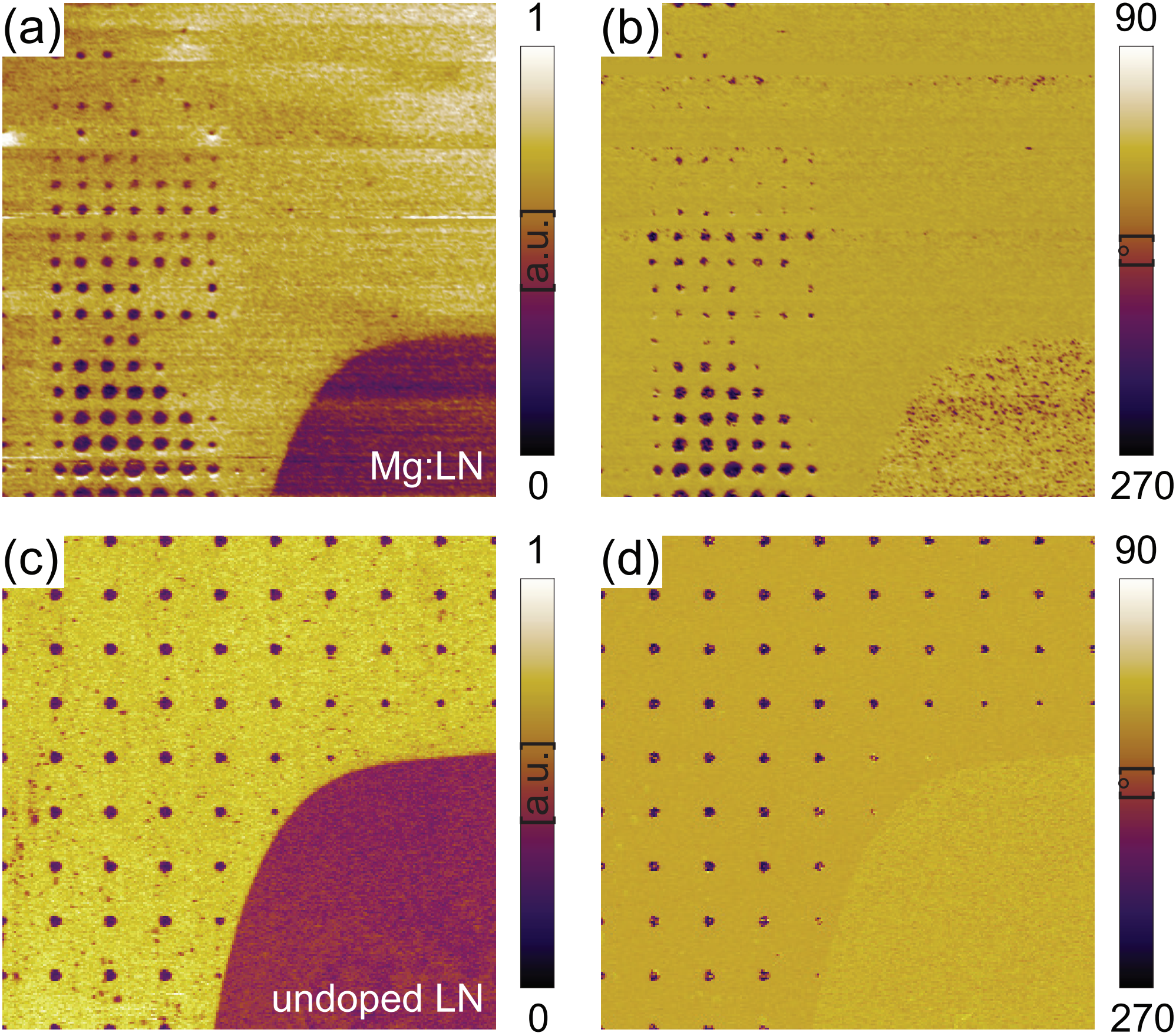
(a)
Mg:LN
1
[a.u.]
0
(b)
90
[°]
270
(c)
undoped LN
1
[a.u.]
0
(d)
90
[°]
270

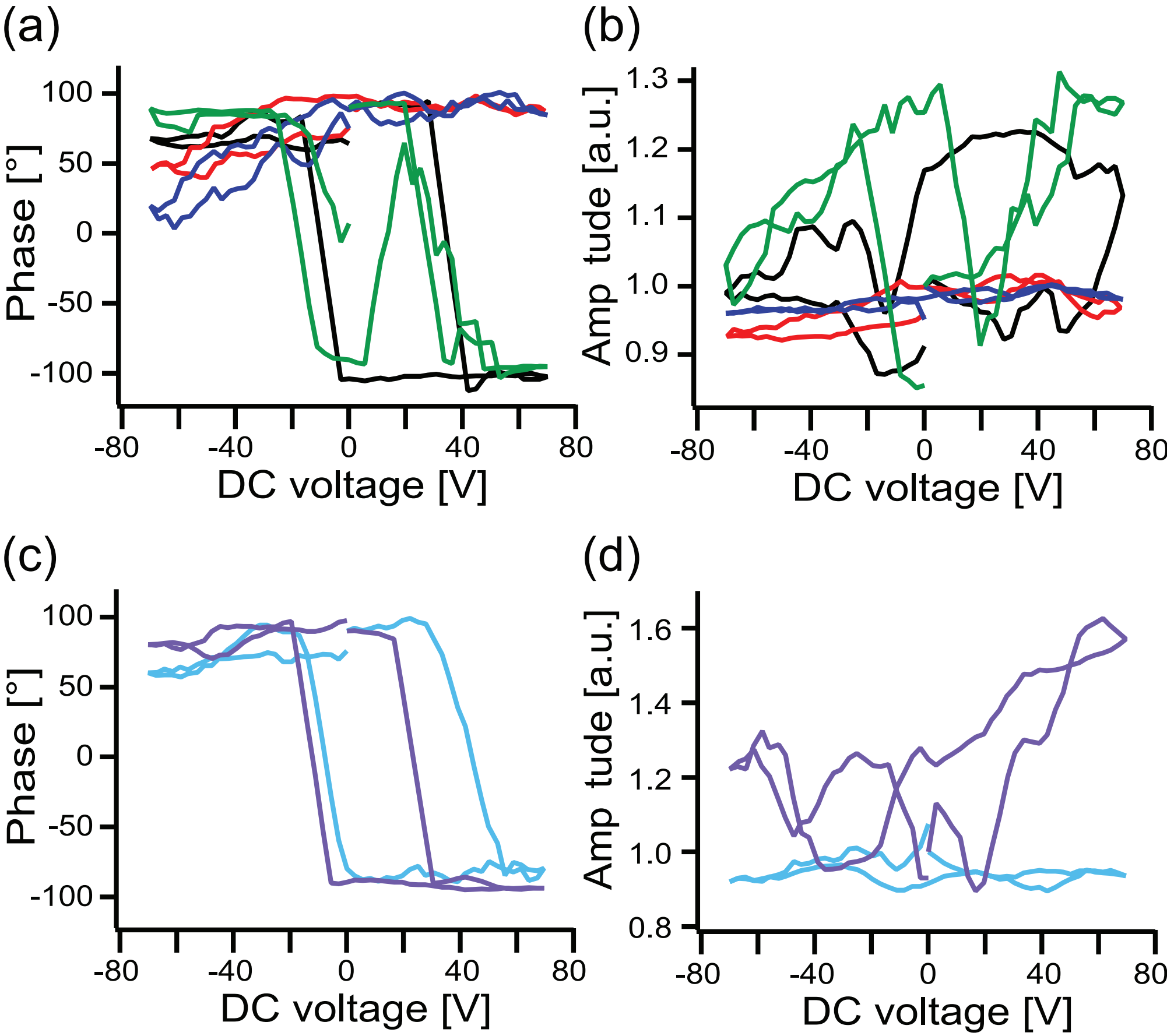
(a)
Phase [°]
100
50
0
-50
-100
-80
-40
0
40
80
DC voltage [V]
(b)
Amp tude [a.u.]
1.3
1.2
1.1
1.0
0.9
-80
-40
0
40
80
DC voltage [V]
(c)
Phase [°]
100
50
0
-50
-100
-80
-40
0
40
80
DC voltage [V]
(d)
Amp tude [a.u.]
1.6
1.4
1.2
1.0
0.8
-80
-40
0
40
80
DC voltage [V]

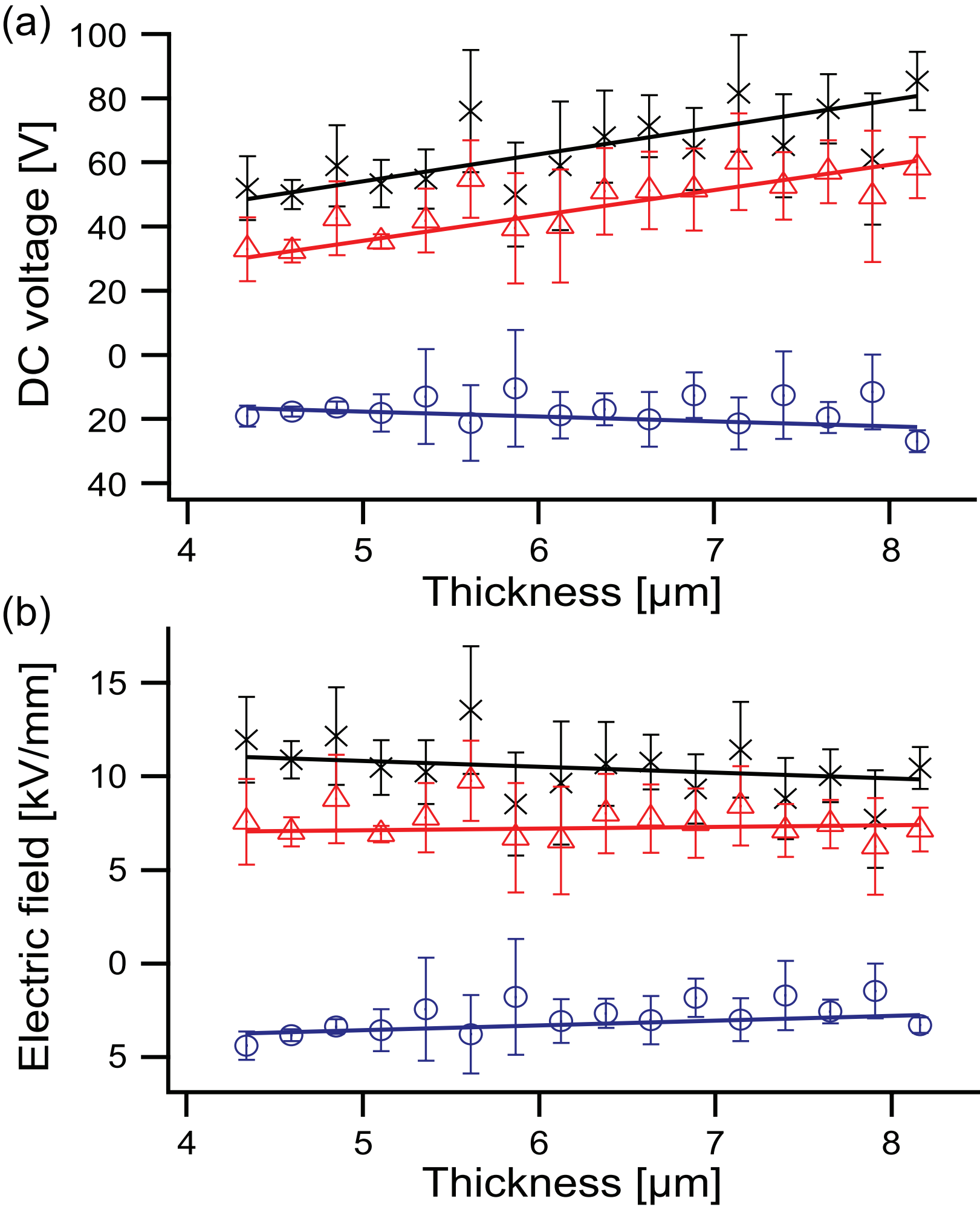
(a)
100
80
60
40
20
0
20
40
DC voltage [V]
4
5
6
7
8
Thickness [μm]
(b)
15
10
5
0
5
Electric field [kV/mm]
4
5
6
7
8
Thickness [μm]

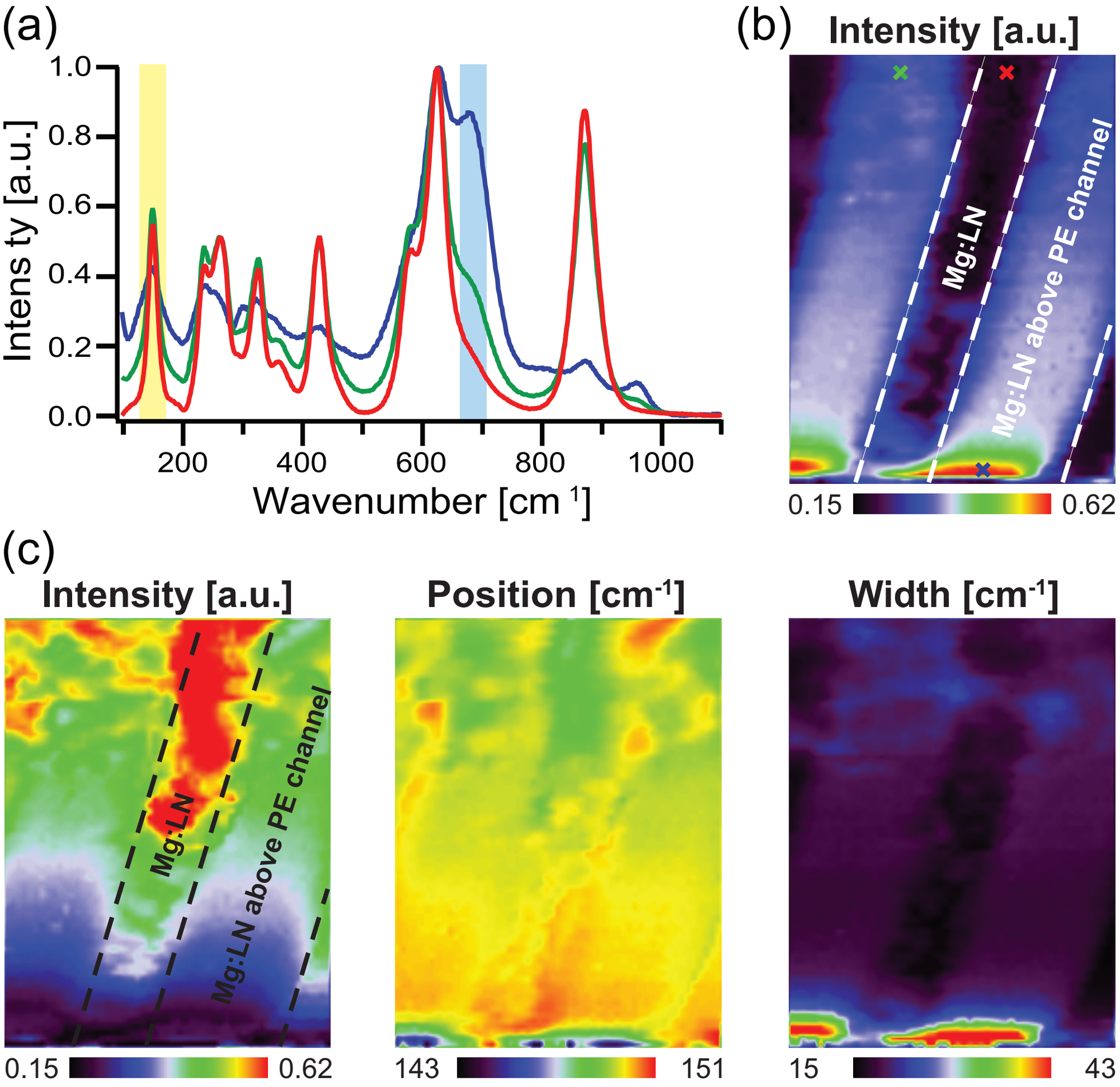
(a)
Intens ty [a.u.]
1.0
0.8
0.6
0.4
0.2
0.0
200
400
600
800
1000
Wavenumber [cm 1]
(b)
Intensity [a.u.]
Mg:LN
Mg:LN above PE channel
0.15
0.62
(c)
Intensity [a.u.]
Mg:LN
Mg:LN above PE channel
0.15
0.62
Position [cm-1]
143
151
Width [cm-1]
15
43